



Signal-off photoelectrochemical determination of miRNA-21 using aptamer-modified $\text{In}_2\text{O}_3@ \text{Cu}_2\text{MoS}_4$ nanocomposite

Ling Dan Yu¹ · Yu Xia Wen¹ · Xing Yue Zhang¹ · Nian Bing Li¹ · Hong Qun Luo¹

Received: 31 May 2020 / Accepted: 30 August 2020 / Published online: 12 September 2020
© Springer-Verlag GmbH Austria, part of Springer Nature 2020

Abstract

$\text{In}_2\text{O}_3@ \text{Cu}_2\text{MoS}_4$ nanocomposite with superior photoelectrochemical (PEC) performance is used for the first time as a photoactivity material, and a signal-off PEC biosensing platform for miRNA detection has been successfully constructed. Firstly, the Cu_2MoS_4 nanosheets are synthesized by a hydrothermal method, and then, the homogeneous In_2O_3 nanoparticles (In_2O_3 NPs) are synthesized by calcination in the air. The $\text{In}_2\text{O}_3@ \text{Cu}_2\text{MoS}_4$ nanocomposite is constructed with the Cu_2MoS_4 nanosheets as matrix and In_2O_3 NPs as sensitizer through a layer-by-layer assembly strategy. The nanocomposite with a tight interface and the matched band structure restrains the electron-hole pair recombination. Under visible light (400–700 nm), the nanocomposite exhibits a strong initial signal. With the catalyzed hairpin assembly, dozens of PbS quantum dots (QDs) are introduced on the surface of an electrode, significantly reducing the photocurrent of n-type $\text{In}_2\text{O}_3@ \text{Cu}_2\text{MoS}_4$. Since PbS QDs can compete with the nanocomposite for light energy and electron donors, the signal decreased. Under optimal conditions, the biosensor manifests a broad linear range (1 fM–1 nM) and a low detection limit of about 0.57 fM, at a working potential of 0 V (vs. Ag/AgCl). The recovery of spiked human serum is between 94.0 and 102%, and the relative standard deviation (RSD) is between 1.3 and 2.7%. Therefore, the as-fabricated biosensor exhibits a potential for the determination of miRNA-21 in practical applications.

Keywords Photoelectrochemical biosensor · $\text{In}_2\text{O}_3@ \text{Cu}_2\text{MoS}_4$ nanocomposite · PbS QDs · Aptasensor

Introduction

In recent years, miRNAs have gained increasing attention of researchers, as miRNAs play an important regulatory role in a series of gene expressions [1, 2]. The expression of miRNAs is closely related to the diagnosis, treatment, and physiological processes in the organism [3]. In addition, according to the report, various momentous diseases were interrelated with the aberrant expressions of miRNAs, such

as cancers, malignancies, and heart disease [4, 5]. Various techniques have been exploited to detect miRNAs, for instance, colorimetry [6], fluorescence [7, 8], electrochemiluminescence (ECL) [9], electrochemistry [10, 11], and capillary electrophoresis [12]. However, due to the instability of microRNA, low content and short length, and similar sequences in the microRNA family, microRNA detection is more difficult. In order to improve the sensitivity, Bharti et al. designed a carboxylated graphene oxide decorated with gold-platinum bimetallic nanoparticles electrochemical bioelectrode for rapid detection of microRNA-21. The sensor has a wide linear response from 1 fM to 1 μM microRNA-21 with a detection limit of 1 fM [13]. Chen et al. developed a self-assembled DNA nanopompon for microRNA detection with the detection limit of 0.8 pM [14]. There is no doubt that some tremendous progress has been made in the detection of miRNAs. These analytical methods still have some non-negligible drawbacks, such as high background signals, heavy equipment, and cumbersome operation. Therefore, it is significant to develop a simple and sensitive biosensor for miRNA detection.

Electronic supplementary material The online version of this article (<https://doi.org/10.1007/s00604-020-04540-z>) contains supplementary material, which is available to authorized users.

✉ Nian Bing Li
linb@swu.edu.cn

✉ Hong Qun Luo
luohq@swu.edu.cn

¹ School of Chemistry and Chemical Engineering, Southwest University, 2, Tiansheng Road, BeiBei District, Chongqing 400715, People's Republic of China

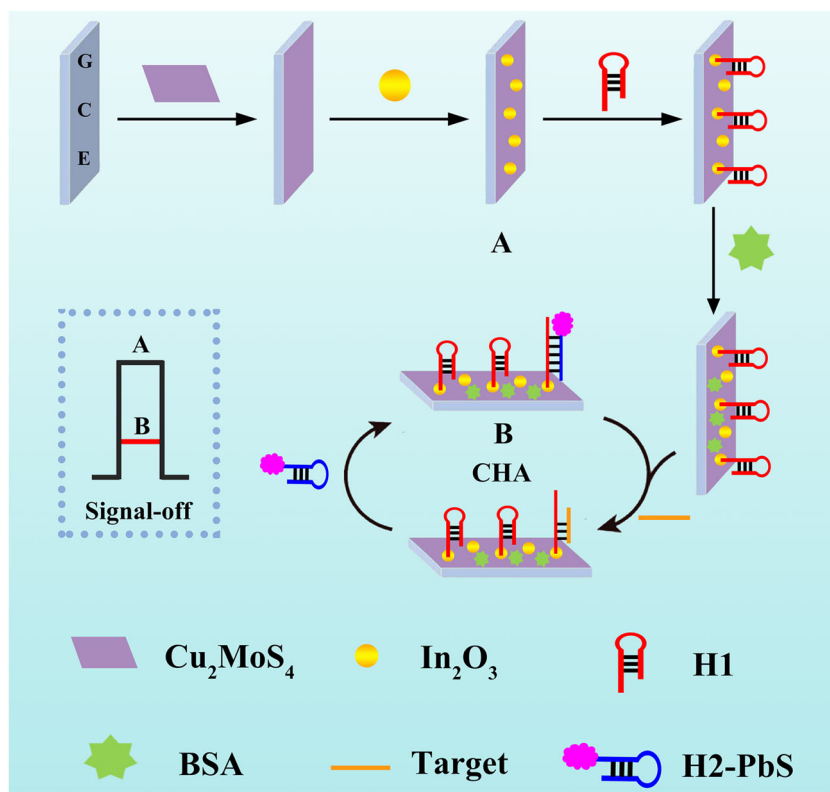
Photoelectrochemical (PEC) sensing technology, an emerged and innovative technology, has gained considerable attention, due to its unparalleled merits of rapid response, simple operation, good stability, and easy miniaturization [15]. Undoubtedly, photoactive materials are an important part of PEC biosensors. So far, various semiconductor materials, including Bi_2S_3 [16], BiOI [17], WO_3 [18], CuInS_2 [19], and Cu_2MoS_4 [20], have received more attention. Among them, Cu_2MoS_4 is a typical layered semiconductor with abundant resources, no pollution to the soil, and low cost [21]. However, Cu_2MoS_4 suffers from the narrow band gap (~ 1.6 eV) which has low photocurrent conversion efficiency and high electron-hole recombination rate [22]. In a previous research, Chi et al. developed a sensitized graphene/ Cu_2MoS_4 composite material based on manganese-doped CdS for the detection of cardiac troponin I, and $\text{CdS}:\text{Mn}$ nanoparticles expand the light absorption range of Cu_2MoS_4 and suppress the recombination of electron-hole pairs. In order to overcome the photocurrent intensity of Cu_2MoS_4 , some compositing or doping methods have been introduced to enlarge its light absorption range.

Traditional optoelectronic materials, such as ZnO and TiO_2 , have high photoinduced electron-hole-pair recombination rate and primary absorption in the ultraviolet spectrum, which severely hinders their practical application under visible light. As an n-type semiconductor with a band gap of ~ 2.7 eV, In_2O_3 is considered a viable candidate for visible light

catalyst. However, there are few applications in photoelectrochemical sensing. More importantly, the energy band matching between Cu_2MoS_4 and In_2O_3 promotes the separation of photo-generated electrons and holes, which is conducive to electron transfer.

Herein, the $\text{In}_2\text{O}_3@ \text{Cu}_2\text{MoS}_4$ nanocomposite was prepared by continuous hydrothermal, calcination, and layer-by-layer assembly method. To our knowledge, $\text{In}_2\text{O}_3@ \text{Cu}_2\text{MoS}_4$ nanocomposite has not been reported and has not been used for sensors. Compared with the previous methods, this synthesis method is simple. $\text{In}_2\text{O}_3@ \text{Cu}_2\text{MoS}_4$ nanocomposite promotes the separation of electron and hole pairs and possesses a stronger photoelectric response. It has great application prospects in PEC sensors. In order to explore a sensitive and high specific strategy to detect miRNA, a “signal-off” PEC biosensor based on $\text{In}_2\text{O}_3@ \text{Cu}_2\text{MoS}_4$ nanocomposite was developed. In this biosensor, PbS quantum dots (PbS QDs) were an effective quencher because PbS QDs can compete for light and electron donors. Scheme 1 describes the preparation process of the PEC biosensor. After modification with the $\text{In}_2\text{O}_3@ \text{Cu}_2\text{MoS}_4$ nanocomposite, thioglycolic acid (TGA) was dripped on the modified electrode. The functionalization of $\text{In}_2\text{O}_3@ \text{Cu}_2\text{MoS}_4$ nanocomposite by TGA introduced the carboxyl groups, which can bind to the hairpin probe (H1) after *N*-(3-(dimethylamino)propyl)-*N'*-ethylcarbodiimide hydrochloride/*N*-hydroxysuccinimide (EDC/NHS) activation. Subsequently, the modified electrode

Scheme 1 The fabrication process of the sensor



was incubated with the target of different concentrations and H2-PbS to generate DNA complexes after blocking the active sites with bovine serum albumin (BSA). Thus, catalyzed hairpin assembly (CHA) was constructed, and the target can carry out the next reaction to achieve the cyclic amplification. The CHA process consists of two hairpin structures (H1 and H2). Hairpin H2 includes a fragment of a sequence complementary to the hairpin H1. In the absence of target, H1 and H2 maintain original hairpin structure in solution. Hairpin H1 contains the recognition sequence of the target. In the presence of target, H1 will fully hybridize with the target miRNA and expand the hairpin structure of H1. Then, H2 hybridizes with the unfolded H1 and replaces the target miRNA according to the mechanism of strand displacement. The H1 sequence hybridizes with the replaced target miRNA again and initiates a strand displacement cycle, thereby introducing PbS QDs into the double-stranded DNA. The CHA process shows great potential in signal amplification, because CHA is a kinetic-controlled reaction that does not require any enzymes to release the target. Therefore, the PEC biosensor exhibited the performance of sensitive response.

Experimental section

Materials and apparatus

Copper(II) chloride dihydrate ($\text{CuCl}_2 \cdot 2\text{H}_2\text{O}$), polyvinylpyrrolidone (PVP), ascorbic acid (AA), and sodium molybdate dihydrate ($\text{Na}_2\text{MoO}_4 \cdot 2\text{H}_2\text{O}$) were obtained from Sigma-Aldrich Co., Ltd. (St. Louis, MO, USA, <http://www.sigmaaldrich.com/>). Other reagents and apparatus used are provided in the Electronic Supporting Material.

Preparation of Cu_2MoS_4 nanosheets and In_2O_3 nanoparticles

According to reference [20], Cu_2MoS_4 nanosheets were prepared by a simple hydrothermal method with slight changes. In addition, In_2O_3 nanoparticles (In_2O_3 NPs) are prepared by calcination in air. The detailed processes are shown in the Electronic Supporting Material.

PEC measurements

PEC detection was carried out in the phosphate buffer ($0.1 \text{ mol L}^{-1} \text{ NaH}_2\text{PO}_4 \cdot 2\text{H}_2\text{O}$, $0.1 \text{ mol L}^{-1} \text{ Na}_2\text{HPO}_4 \cdot 12\text{H}_2\text{O}$, and $0.1 \text{ mol L}^{-1} \text{ KCl}$, pH 7.4) containing 0.1 M AA. The applied potential was 0 V with $400\text{--}700 \text{ nm}$ light as an excitation source and a light intensity of 20 mW m^{-2} . All electrochemical experiments were performed with a classical three-electrode system including a platinum wire counter

electrode, a modified glassy carbon working electrode ($\Phi = 3 \text{ mm}$), and an Ag/AgCl reference electrode.

Fabrication of PEC sensor

In this study, a glassy carbon electrode (GCE) surface with a diameter of 3 mm was thoroughly rinsed with alumina powder of $0.05 \mu\text{m}$ and then sonicated for 2 min with water and ethanol. Meanwhile, 2 mg of Cu_2MoS_4 was dispersed in 1 mL ultrapure water and $10 \mu\text{L}$ of Nafion by sonication to obtain a suspension. Following that, $10 \mu\text{L}$ of the suspension was coated on the cleaning GCE and dried at room temperature. Then, the resulting electrode was anchored on $10 \mu\text{L}$ of In_2O_3 suspension (2 mg/mL) and then evaporation in the air. After that, $10 \mu\text{L}$ of TGA (3 mM) was incubated on the modified electrode overnight. After washing with water, $10 \mu\text{L}$ of the mixed solution containing 10 mM EDC and 20 mM NHS was dropped on the $\text{TGA}/\text{In}_2\text{O}_3/\text{Cu}_2\text{MoS}_4/\text{GCE}$ electrode to activate the modified electrode for 1 h , followed by washing with water. Whereafter, $10 \mu\text{L}$ of hairpin H1 ($2 \mu\text{M}$) was added to the modified electrode and incubated in a refrigerator overnight. The physically adsorbed H1 was eliminated by washing with water. After blocking with 1% BSA for 1 h , the $\text{BSA}/\text{H1}/\text{In}_2\text{O}_3/\text{Cu}_2\text{MoS}_4/\text{GCE}$ was incubated with $10 \mu\text{L}$ of target and $10 \mu\text{L}$ of H2-PbS at $37 \text{ }^\circ\text{C}$ for 2 h .

Results and discussion

Characterization of Cu_2MoS_4 nanosheets and In_2O_3 NPs

The morphology of Cu_2MoS_4 nanosheets at different magnifications was investigated by a scanning electron microscope (SEM) in Fig. 1a, b, and c. As can be seen from these pictures, Cu_2MoS_4 nanosheets formed as a square nanoplate with a size of about 0.8 to $1.1 \mu\text{m}$. In Fig. 1d, indium mixed-ligand metal-organic frameworks (MIL-68 (In)) was rod-shaped and had a relatively uniform size, which was about $1.1 \mu\text{m}$. MIL-68 (In) derived In_2O_3 NPs presented homogeneous aggregates with a size of about 20 nm (Fig. 1e, f). The elemental mapping certified the appearance of Cu, Mo, S, In, and O elements in the nanomaterial (Fig. S1). In addition, the characterization of PbS QDs is presented in the Electronic Supporting Material (Fig. S2).

In addition, the crystal structure of the nanomaterials was verified by X-ray power diffraction (XRD). As illustrated in Fig. 2a, the diffraction peaks of Cu_2MoS_4 were consistent with the literature [22], meaning that the Cu_2MoS_4 has been successfully synthesized. Similarly, all peaks appearing in the In_2O_3 NPs were consistent with the literature [23]. In Fig. 2b, UV-vis diffuse reflectance spectrum (DRS) of In_2O_3 exhibits poor photo-absorption. Nevertheless, Cu_2MoS_4 is a broaden

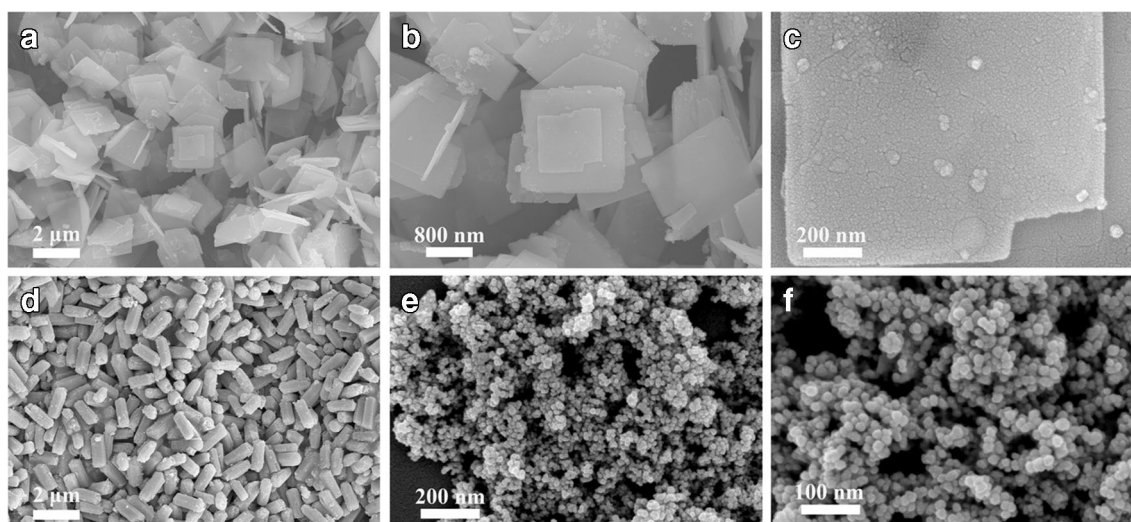


Fig. 1 SEM images of Cu₂MoS₄ (a–c), MIL-68(In) (d), and In₂O₃ NPs (e, f)

absorption range in the visible light. The XPS spectra and optical band gaps of Cu₂MoS₄ and In₂O₃ materials are shown in the Electronic Supporting Material (Figs. S3–S5).

PEC and electrochemical impedance spectroscopy characterization of the prepared materials

The *i*-*t* curves were used to investigate the PEC properties of Cu₂MoS₄, In₂O₃, and Cu₂MoS₄/In₂O₃. As shown in Fig. 3a, compared with Cu₂MoS₄/GCE and In₂O₃/GCE, the photocurrent signal of In₂O₃/Cu₂MoS₄/GCE is supreme. The photocurrent of Cu₂MoS₄/GCE is the second, and that of In₂O₃/GCE is the weakest. This demonstrated that the combination of Cu₂MoS₄ and In₂O₃ can suppress the recombination of photo-generated electron and hole efficiently, thereby improving the photoelectric signal. In addition, the Nyquist plots of the materials are depicted in Fig. 3b. A total of 5 mM [Fe(CN)₆]^{3-/4-} solution is used as the electrolyte for testing. The semicircle diameter of the bare GCE exhibits the smallest. As expected, after Cu₂MoS₄ immobilization, the diameter changes sharply, which can

be interpreted to poor electron transfer capability of semiconductor materials. Whereas, after In₂O₃ loaded on the electrodes, the diameter of the semicircle is extremely reduced, which can be attributed to two materials with well-matched band structure and the rapid charge transfer.

Feasibility of the signal amplification method

To verify the cycling process, polyacrylamide gel electrophoresis (PAGE) analysis was used to assess the feasibility of the method (Fig. S6). The bands of lanes 1–3 show H1, H2, and the target, respectively. As expected, the H1/H2 mixture showed H1 and H2 monomer bands, suggesting that CHA amplification was prohibited in the absence of miRNA-21 (lane 5). When the target is added, H1 can form a hybrid band with the target (lane 4), while lane 6 clearly shows a lower electrophoretic mobility band, indicating that the CHA circuit has been successfully assembled. Consequently, the above results signify that the design of CHA amplification is feasible.

Fig. 2 a XRD and b the UV–vis DRS of Cu₂MoS₄ and In₂O₃

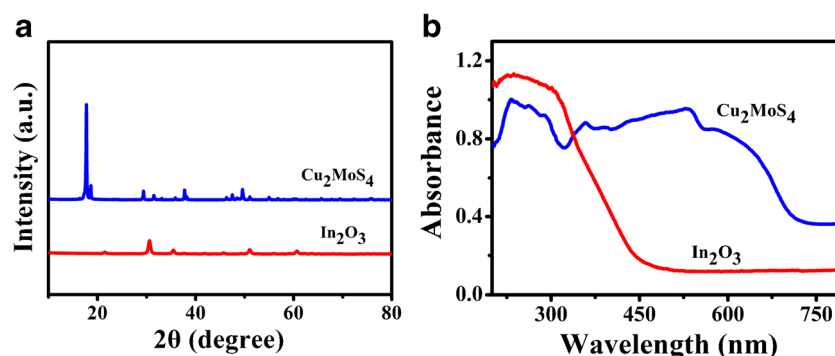
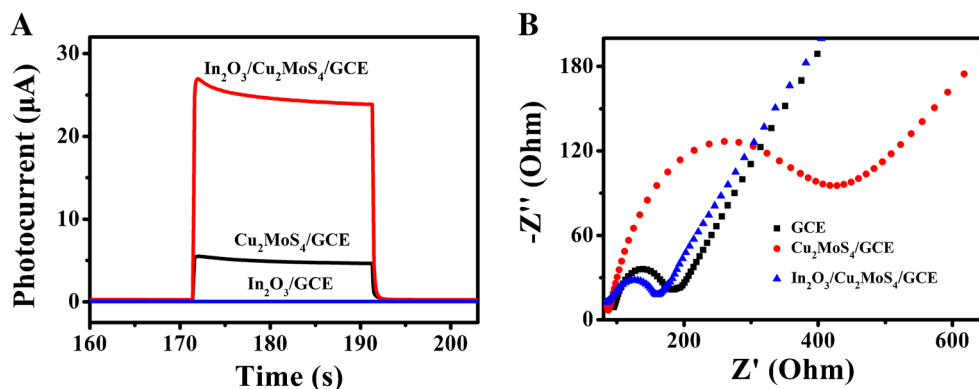


Fig. 3 **a** Photocurrent characterization of $\text{In}_2\text{O}_3/\text{Cu}_2\text{MoS}_4/\text{GCE}$, $\text{Cu}_2\text{MoS}_4/\text{GCE}$, and $\text{In}_2\text{O}_3/\text{GCE}$. **b** Nyquist plots of the bare GCE, $\text{Cu}_2\text{MoS}_4/\text{GCE}$, and $\text{In}_2\text{O}_3/\text{Cu}_2\text{MoS}_4/\text{GCE}$



Detection mechanism

In addition, the photocurrent generation and reduction mechanism of the sensor are proposed in Scheme 2. Since Nafion cannot be used for In_2O_3 solution during the process of fixing the material, the Cu_2MoS_4 is modified first. In addition, the electrons in the n-type semiconductor move toward the positive potential, so the sequence shown in Scheme 2 is adopted. As can be seen from Scheme 2a, photo-generated electrons of Cu_2MoS_4 are excited from the VB to the CB, and photo-generated holes are generated in VB under the visible light. Therefore, the photo-generated electrons in the CB of Cu_2MoS_4 were injected to the CB of In_2O_3 and then transferred to the electrode surface, generating an anode signal. Then, the photo-generated holes in the VB of In_2O_3 transfer to the VB of Cu_2MoS_4 , and the holes in the VB of Cu_2MoS_4 were further consumed by the AA, which existed in the electrolyte. Consequently, the entire process accelerates the migration of photo-generated electrons between two materials, avoiding the recombination of electrons and holes.

As PbS QDs were introduced through the CHA reaction, the photocurrent was reduced (Scheme 2b). Firstly, since $\text{In}_2\text{O}_3@/\text{Cu}_2\text{MoS}_4$ nanocomposite is an n-type semiconductor, the photo-generated electrons will be transferred to the electrode surface to generate an anode photocurrent, so they will not be captured by oxygen. In the presence of p-type PbS QDs, the photo-generated electrons will be transferred to the electrolyte and then captured by dissolved oxygen (electron acceptors) in the solution to form $\text{O}_2^{\cdot-}$ (e), and the photo-generated holes are neutralized with ascorbic acid, which

can decrease the concentration of electron donors in solution mediately [24]. Secondly, the wide absorption of PbS QDs competes with $\text{In}_2\text{O}_3@/\text{Cu}_2\text{MoS}_4$ to absorb light energy, which reduces the light absorption of the $\text{In}_2\text{O}_3@/\text{Cu}_2\text{MoS}_4$ and leads to a reduction in photocurrent [25]. Third, the electron transfer was retarded due to the steric hindrance of PbS QDs, which can also reduce the photocurrent response. Therefore, an effective reduced photocurrent response can be obtained in the presence of PbS QDs.

Characterization of the as-fabricated sensor

To ensure the complete assembly of the electrode, electrochemical cyclic voltammetry (CV) was employed to characterize each step of the construction process. Figure 4a shows curve (i) represents bare GCE with a couple of quasi-reversible redox peaks. After the electrode surface was modified with Cu_2MoS_4 , the signal was obviously reduced (curve ii). Afterwards, the In_2O_3 was anchored; the redox peak current increased sharply, indicating that Cu_2MoS_4 and In_2O_3 have good conductivity and accelerate electron transfer (curve iii). When H1 is attached, the steric resistance of the electrode surface is increased; thus, the redox peak current will have a relatively significant decrease (curve iv). Non-specific recognition sites were blocked with BSA, hindering the transfer of electrons and reducing the redox peak current (curve v). Due to the CHA reaction, many PbS QDs are assembled. As an electron acceptor, the electron transfer on the electrode surface is reduced, and the redox peak current is markedly decreased (curve vi).

Scheme 2 Photocurrent generation mechanism of the biosensor

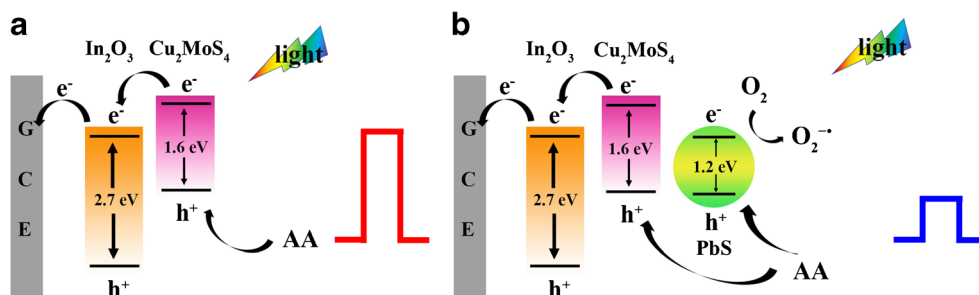


Fig. 4 CV (a) and PEC (b) of electrode assembly at each step: (i) GCE, (ii) $\text{Cu}_2\text{MoS}_4/\text{GCE}$, (iii) $\text{In}_2\text{O}_3/\text{Cu}_2\text{MoS}_4/\text{GCE}$, (iv) after H1 modification, (v) after BSA anchoring, and (vi) after incubation with target and H2-PbS

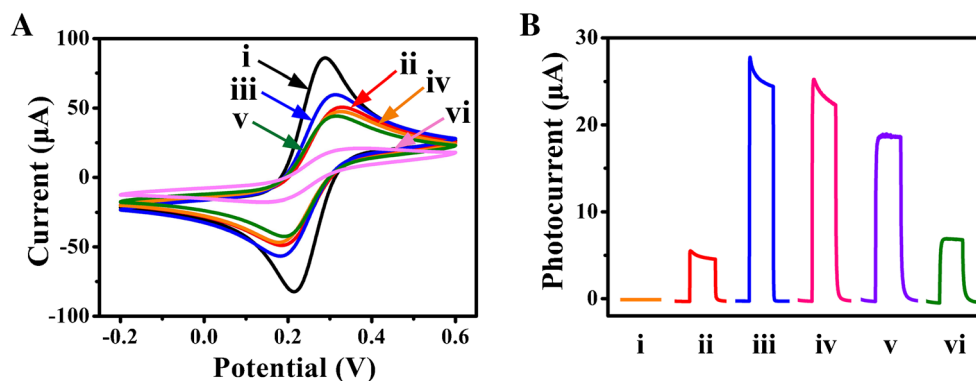


Figure 4b reveals that the bare electrode (curve i) displays a negligible signal. Compared with curve (a), remarkable photocurrent signal is generated after modification of Cu_2MoS_4 (curve ii). This phenomenon can be illustrated as Cu_2MoS_4 itself is an outstanding photoactive material, which can generate photo-generated electrons under the excitation of light. At the same time, as In_2O_3 is modified on the electrode of Cu_2MoS_4 , the photocurrent signal increases sharply (curve iii). This is because the band structure of $\text{Cu}_2\text{MoS}_4/\text{In}_2\text{O}_3$ is well matched, which can greatly enhance the photoelectric conversion under visible light irradiation. After incubation with H1, the photocurrent decreased to some extent (curve iv), which was due to the spatial inhibition effect. BSA then blocked non-specific binding sites and increased steric hindrance, so photocurrent decreased (curve v). When H2-PbS is

modified, the photocurrent is significantly reduced (curve vi). This result fully proves the successful construction of PEC biosensors.

Effective surface area

To investigate the effect of various fabricated materials on electrode surface, CV responses were measured at different scan rates from 10 to 100 mV/s in 5 mM $[\text{Fe}(\text{CN})_6]^{3-/4-}$ solution. The calculation results are presented in the ESM (Table S1 and Fig. S7), which can be used to calculate the current density of different electrodes.

Optimization of experimental conditions

To improve the analytical performance of the designed PEC sensor, the experimental conditions were optimized,

Fig. 5 a Photocurrent response of different concentrations target (miRNA-21) (0 fM, 1 fM, 10 fM, 100 fM, 1 pM, 10 pM, 100 pM, 1 nM). b Calibration curves for different concentrations of target. c The stability test of the sensor. d The PEC photocurrent intensity responses to blank, miRNA-141, miRNA-155, miRNA-203a, and miRNA-21 (from 1 to 5) on the photocurrent responses

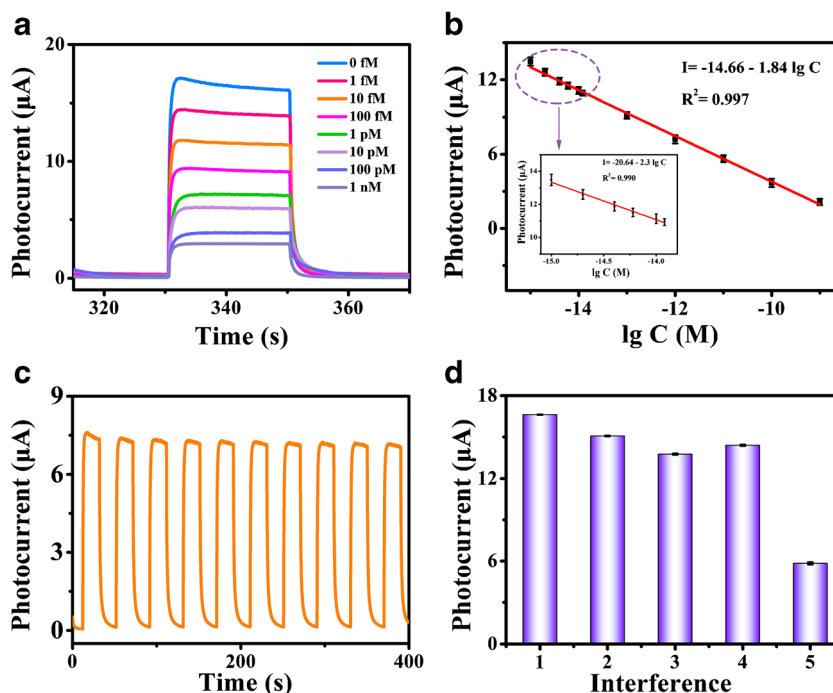


Table 1 Performance comparison of microRNA-21 detection by different detection methods

Method	Linear range (pM)	Detection limit (fM)	Reference
ECL	1.0×10^{-2} –1.0	10.0	[26]
ECL	1.0×10^{-4} –100.0	3.4×10^{-3}	[27]
Fluorescence	1.0×10^{-2} – 1.0×10^3	10.0	[28]
Electrochemistry	1.0×10^{-3} –10.0	1.0	[29]
Electrochemistry	1.0×10^{-5} – 1.0×10^{-2}	5.0×10^{-3}	[30]
Electrochemistry	0.1– 1.0×10^3	68.0	[31]
PEC	1.0×10^{-3} – 1.0×10^3	0.57	This work

including (a) the concentration of AA, (b) the incubation time of H₂-PbS QDs, and (c) the concentration of H₂ (Fig. S8). Details have been discussed in the ESM. The electrolyte AA (0.1 M), 2 μ M H₂ probe, and 2-h incubation time were selected for response studies.

Analytical performance

The photocurrent of PEC biosensor is directly related to the concentration of microRNA-21. As depicted in Fig. 5a, as the target concentration increased, the photocurrent is reduced, which is attributed to PbS QDs assembled on the electrode.

Furthermore, the photocurrent response had a clear linear relationship with the concentration of microRNA-21 (Fig. 5b). The linear equation is $I = -14.66 - 1.84 \lg c$, and the correlation coefficient is 0.997. The limit of detection for microRNA-21 was about 0.57 fM ($3\sigma/S$, where σ denotes the standard deviation of 8 tests for blank sample and S refers to the slope of the linear equation; Table S2), which is comparable with previous reported biosensors for microRNA-21 detection (Table 1).

As is seen from Fig. 5c, after switching on and off the light for dozens of times within 400 s, the photocurrent has not decreased significantly, indicating that the sensor has excellent stability. To probe selectivity of the prepared sensor, blank group and various miRNAs were used to evaluate specificity. As shown in Fig. 5d, in the presence of various targets: miRNA-141 (10 pM), miRNA-155 (10 pM), miRNA-203a (10 pM), compared with the blank group, the photocurrent signal did not change significantly, while 10 pM miRNA-21 significantly reduced the PEC signal, indicating the good selectivity for the sensor.

Analysis application in real samples

To confirm the practicability of the sensor, standard addition method was carried out. First, the blood samples were centrifuged and the supernatant serum is taken out. The serum was diluted fivefold with phosphate buffer (0.1 M pH 7.4). No miRNA-21 was detected in unspiked serum in this method. Then, different concentrations of microRNA-21 (5 μ L) within the linear range were added to the serum (5 μ L). Other

experimental conditions remain unchanged. The photocurrent was recorded by visible light irradiation at an applied potential of 0 V. The lamp (20 mW m⁻², 400–700 nm) was used as irradiation source in the PEC test. From the results in Table S3, the recovery was between 94.0 and 102%, and relative standard deviation (RSD) was between 1.25 and 2.72%, indicating that the constructed biosensor had promising analytical applications in clinical research. However, the modification process of the sensor is complicated and needs further improvement.

Conclusions

The In₂O₃@Cu₂MoS₄ nanomaterials were employed as the photoactive material for the first time. Due to the matched band-edge levels, the photoelectric conversion of the nanomaterials is significantly enhanced, which can effectively suppress the recombination of photo-generated electrons. A new type of optoelectronic active material was developed, and with the aid of the circular amplification strategy of CHA, the detection range and the application prospect of the sensor were improved. Therefore, compared with the traditional PEC sensing method of “signal-off,” the developed photoelectric-based materials can effectively improve the sensitivity and selectivity of the sensor. Obviously, this strategy provides a new method for biological analysis.

Funding This work was financially supported by the National Natural Science Foundation of China (No. 21675131) and the Natural Science Foundation of Chongqing (CSTC-2015jcyjB50001).

Compliance with ethical standards

Conflict of interest The authors declare that they have no conflict of interest.

References

- Lu SS, Wang S, Zhao JH, Sun J, Yang XR (2017) Fluorescence light-up biosensor for microRNA based on the distance-dependent photoinduced electron transfer. *Anal Chem* 89:8429–8436. <https://doi.org/10.1021/acs.analchem.7b01900>

2. Lu LP, Wang JX, Miao WJ, Wang XY, Guo GS (2019) Electrogenerated chemiluminescence biosensor with a tripod probe for the highly sensitive detection of microRNA. *Anal Chem* 91: 1452–1459. <https://doi.org/10.1021/acs.analchem.8b04271>
3. Ye C, Wang MQ, Luo HQ, Li NB (2017) Label-free photoelectrochemical “off-on” platform coupled with g-wire-enhanced strategy for highly sensitive microRNA sensing in cancer cells. *Anal Chem* 89:11697–11702. <https://doi.org/10.1021/acs.analchem.7b03150>
4. Zhou MX, Teng XC, Li Y, Deng RJ, Li JH (2019) Cascade transcription amplification of RNA aptamer for ultrasensitive microRNA detection. *Anal Chem* 91:5295–5302. <https://doi.org/10.1021/acs.analchem.9b00124>
5. Lu J, Wang J, Hu XL, Gyimah E, Yakubu S, Wang K, Wu XY, Zhang Z (2019) Electrochemical biosensor based on tetrahedral DNA nanostructures and g-quadruplex-hemin conformation for the ultrasensitive detection of microRNA-21 in serum. *Anal Chem* 91:7353–7359. <https://doi.org/10.1021/acs.analchem.9b01133>
6. Ling Y, Gao ZF, Zhou Q, Li NB, Luo HQ (2015) Multidimensional optical sensing platform for detection of heparin and reversible molecular logic gate operation based on the phloxine B/polyethyleneimine system. *Anal Chem* 87:1575–1581. <https://doi.org/10.1021/ac504023b>
7. Dong HF, Zhang J, Ju HX, Lu HT, Wang SY, Jin S, Hao KH, Du HW, Zhang XJ (2012) Highly sensitive multiple microRNA detection based on fluorescence quenching of graphene oxide and isothermal strand-displacement polymerase reaction. *Anal Chem* 84: 4587–4593. <https://doi.org/10.1021/ac300721u>
8. Yang L, Liu CH, Ren W, Li ZP (2012) Graphene surface-anchored fluorescence sensor for sensitive detection of microRNA coupled with enzyme-free signal amplification of hybridization chain reaction. *ACS Appl Mater Interfaces* 4:6450–6453. <https://doi.org/10.1021/am302268t>
9. Liu W, Chen AY, Li SK, Peng KF, Chai YQ, Yuan R (2019) Perylene derivative/luminol nanocomposite as a strong electrochemiluminescence emitter for construction of an ultrasensitive microRNA biosensor. *Anal Chem* 91:1516–1523. <https://doi.org/10.1021/acs.analchem.8b04638>
10. Tian L, Qian K, Qi JX, Liu QY, Yao C, Song W, Wang YH (2018) Gold nanoparticles superlattices assembly for electrochemical biosensor detection of microRNA-21. *Biosens Bioelectron* 99:564–570. <https://doi.org/10.1016/j.bios.2017.08.035>
11. Su S, Cao WF, Liu W, Lu ZW, Zhu D, Chao J, Weng LX, Wang LH, Fan CH, Wang LH (2017) Dual-mode electrochemical analysis of microRNA-21 using gold nanoparticle-decorated MoS₂ nanosheet. *Biosens Bioelectron* 94:552–559. <https://doi.org/10.1016/j.bios.2017.03.040>
12. Mikova B, Dvorak M, Rysava L, Kuban P (2020) Hollow fiber liquid-phase microextraction at-line coupled to capillary electrophoresis for direct analysis of human body fluids. *Anal Chem* 92: 7171–7178. <https://doi.org/10.1021/acs.analchem.0c00697>
13. Bharti A, Agnihotri N, Prabhakar N (2019) A voltammetric hybridization assay for microRNA-21 using carboxylated graphene oxide decorated with gold-platinum bimetallic nanoparticles. *Mikrochim Acta* 186:185. <https://doi.org/10.1007/s00604-019-3302-3>
14. Chen ND, Li JY, Feng XZ, Yang YP, Zhu L, Chen XM, Liu X, Li Y, Wang CC, Xia LG (2020) Label-free and self-assembled fluorescent DNA nanopompom for determination of miRNA-21. *Mikrochim Acta* 187:432. <https://doi.org/10.1007/s00604-020-04377-6>
15. Ge L, Li HN, Du XJ, Zhu MY, Chen W, Shi TY, Hao N, Liu Q, Wang K (2018) Facile one-pot synthesis of visible light-responsive BiPO₄/nitrogen doped graphene hydrogel for fabricating label-free photoelectrochemical tetracycline aptasensor. *Biosens Bioelectron* 111:131–137. <https://doi.org/10.1016/j.bios.2018.04.008>
16. Wang FX, Ye C, Mo S, Liao LL, Luo HQ, Li NB (2019) A novel photoelectrochemical sensing platform based on Fe₂O₃@Bi₂S₃ heterojunction for an enzymatic process and enzyme activity inhibition reaction. *Sensors Actuators B Chem* 288:202–209. <https://doi.org/10.1016/j.snb.2019.02.121>
17. Yan K, Liu Y, Yang YH, Zhang JD (2015) A cathodic “signal-off” photoelectrochemical aptasensor for ultrasensitive and selective detection of oxytetracycline. *Anal Chem* 87:12215–12220. <https://doi.org/10.1021/acs.analchem.5b03139>
18. Han QZ, Wang RY, Xing B, Zhang T, Khan MS, Wu D, Wei Q (2018) Label-free photoelectrochemical immunoassay for CEA detection based on CdS sensitized WO₃@BiOI heterostructure nanocomposite. *Biosens Bioelectron* 99:493–499. <https://doi.org/10.1016/j.bios.2017.08.034>
19. Liu C, Zhao L, Liang DX, Zhang XR, Song WL (2019) An CuInS₂ photocathode for the sensitive photoelectrochemical determination of microRNA-21 based on DNA-protein interaction and exonuclease III assisted target recycling amplification. *Mikrochim Acta* 186: 692. <https://doi.org/10.1007/s00604-019-3804-z>
20. Chen WX, Chen HP, Zhu HT, Gao QQ, Luo J, Wang Y, Zhang S, Zhang K, Wang CM, Xiong YJ, Wu YF, Zheng XS, Chu WS, Song L, Wu ZY (2014) Solvothermal synthesis of ternary Cu₂MoS₄ nanosheets: structural characterization at the atomic level. *Small* 10:4637–4644. <https://doi.org/10.1002/smll.201400752>
21. Ma N, Wei B, Cao WL, Gao H, Xu LL (2017) Carbon dots/Cu₂MoS₄ nanosheets hybrids with efficient photoelectrochemical performance. *Mater Lett* 197:79–82. <https://doi.org/10.1016/j.matlet.2017.03.101>
22. Chi HT, Han QZ, Chi TH, Xing B, Ma N, Wu D, Wei Q (2019) Manganese doped CdS sensitized graphene/Cu₂MoS₄ composite for the photoelectrochemical immunoassay of cardiac troponin I. *Biosens Bioelectron* 132:1–7. <https://doi.org/10.1016/j.bios.2019.02.048>
23. Feng YX, Yan T, Wu TT, Zhang N, Yang QQ, Sun M, Yan LG, Du B, Wei Q (2019) A label-free photoelectrochemical aptasensing platform base on plasmon Au coupling with MOF-derived In₂O₃@g-C₃N₄ nanoarchitectures for tetracycline detection. *Sensors Actuators B Chem* 298:126817. <https://doi.org/10.1016/j.snb.2019.126817>
24. Li MJ, Zheng YN, Liang WB, Yuan R, Chai YQ (2017) Using p-type PbS quantum dots to quench photocurrent of fullerene-Au NP@MoS₂ composite structure for ultrasensitive photoelectrochemical detection of ATP. *ACS Appl Mater Interfaces* 9:42111–42120. <https://doi.org/10.1021/acsami.7b13894>
25. Dai WX, Zhang L, Zhao WW, Yu XD, Xu JJ, Chen HY (2017) Hybrid PbS quantum dot/nanoporous NiO film nanostructure: preparation, characterization, and application for a self-powered cathodic photoelectrochemical biosensor. *Anal Chem* 89:8070–8078. <https://doi.org/10.1021/acs.analchem.7b01557>
26. Liao YH, Huang R, Ma ZK, Wu YX, Zhou XM, Xing D (2014) Target-triggered enzyme-free amplification strategy for sensitive detection of microRNA in tumor cells and tissues. *Anal Chem* 86: 4596–4604. <https://doi.org/10.1021/ac5007427>
27. Sun MF, Liu JL, Chai YQ, Zhang J, Tang Y, Yuan R (2019) Three-dimensional cadmium telluride quantum dots-DNA nanoreticulation as a highly efficient electrochemiluminescent emitter for ultrasensitive detection of microRNA from cancer cells. *Anal Chem* 91:7765–7773. <https://doi.org/10.1021/acs.analchem.9b01185>
28. Duan RX, Zuo XL, Wang ST, Quan XY, Chen DL, Chen ZF, Jiang L, Fan CH, Xia F (2013) Lab in a tube: ultrasensitive detection of microRNAs at the single-cell level and in breast cancer patients using quadratic isothermal amplification. *J Am Chem Soc* 135: 4604–4607. <https://doi.org/10.1021/ja311313b>

29. Lin MH, Wen YL, Li LY, Pei H, Liu G, Song HY, Zuo XL, Fan CH, Huang Q (2014) Target-responsive, DNA nanostructure-based E-DNA sensor for microRNA analysis. *Anal Chem* 86:2285–2288. <https://doi.org/10.1021/ac500251t>
30. Labib M, Khan N, Ghobadloo SM, Cheng J, Pezacki JP, Berezovski MV (2013) Three-mode electrochemical sensing of ultralow microRNA levels. *J Am Chem Soc* 135:3027–3038. <https://doi.org/10.1021/ja308216z>
31. Su S, Hao Q, Yan ZY, Dong RM, Yang R, Zhu D, Chao J, Zhou Y, Wang LH (2019) A molybdenum disulfide@methylene blue nanohybrid for electrochemical determination of microRNA-21, dopamine and uric acid. *Mikrochim Acta* 186:607. <https://doi.org/10.1007/s00604-019-3678-0>

Publisher's note Springer Nature remains neutral with regard to jurisdictional claims in published maps and institutional affiliations.